Ultralight Dark Matter from the Edge of Field Space

Mathias Becker,[1,2,*] Francesco D'Eramo,[1,2,†] and Ville Vaskonen[1,2,3,‡]

[1] *Dipartimento di Fisica e Astronomia, Università degli Studi di Padova, Via Marzolo 8, 35131 Padova, Italy*
[2] *INFN, Sezione di Padova, Via Marzolo 8, 35131 Padova, Italy*
[3] *Keemilise ja bioloogilise füüsika instituut, Rävala pst. 10, 10143 Tallinn, Estonia*

We introduce a novel class of bosonic dark matter candidates that we dub wallions, featuring boundaries in field space. The wallion mass is exponentially suppressed when the separation between boundaries far exceeds their intrinsic width and remains radiatively stable under self-interactions. We study the early-universe evolution of wallions and the associated cosmological signatures. Finally, we show that instanton effects can dynamically generate field-space boundaries and discuss possible experimental probes once the wallion couples to Standard Model fields.

arXiv:2511.09622v1 [hep-ph] 12 Nov 2025

Introduction. The observational evidence for dark matter (DM) [1–7] leaves no doubt about the need for physics beyond the Standard Model (SM). Decades after its first indications, the breadth of empirical evidence is matched only by the diversity of theoretical proposals aiming to explain its microscopic particle nature.

Searches for DM have predominantly targeted weakly interacting massive particles (WIMPs), motivated by their connection to the hierarchy problem [8–10] and by the fact that their relic abundance naturally emerges from thermal freeze-out [11–15]. The persistent absence of WIMP signals in recent years has placed this framework under pressure [16–18]. Meanwhile, an extensive experimental effort [19–30], together with theoretical advances [31–35], has reignited interest in ultralight and extremely weakly coupled bosonic candidates. The QCD axion [36–40], introduced to solve the strong CP problem via the Peccei–Quinn mechanism [41, 42], is a particularly motivated example. WIMPs and axions, two leading DM paradigms with deep connections to open questions in particle physics, delineate two distinct mass regimes: *particle* DM, with masses above the eV scale, and *wave* DM, associated with lighter candidates whose de Broglie wavelengths are macroscopic.

Ultralight wave DM has emerged as a particularly compelling candidate [43–45]. It leaves distinctive imprints in cosmological observables, notably the suppression of small-scale structure [31, 46, 47], and has motivated a new generation of precision laboratory experiments probing its subtle effects [48–53]. On astrophysical scales, ultralight DM can induce striking phenomena such as black hole superradiance [54–58], offering additional avenues to constrain its properties. Theoretical consistency, however, requires an explanation for the origin of such tiny masses and their stability against quantum corrections. The QCD axion provides an instructive example: its mass arises dynamically after confinement, while its smallness is protected by its Nambu–Goldstone nature.

In this Letter, we introduce a novel candidate in the landscape of ultralight DM, the *wallion*, whose mass is naturally protected by limits of its field space. Unlike axions, which live on a compact manifold with periodic boundary conditions, the wallion ϕ roams freely up to a hard boundary. Such frameworks have recently attracted attention in high-energy physics [59–61], where field space itself becomes dynamical. Ref. [59] studied an effective field theory (EFT) with a scalar potential growing exponentially beyond $|\phi| > \bar{\phi}$, rendering $|\phi| = \bar{\phi}$ a genuine *field-space boundary*. Remarkably, this structure preserves its form under quantum corrections.

What makes these scenarios interesting in the context of wave DM? Let us first consider the most extreme, albeit unrealistic, case of a potential with a wall:

$$V_{\rm wall}(\phi) = \begin{cases} 0, & |\phi| < \bar{\phi} \\ \infty, & |\phi| \geq \bar{\phi} \end{cases} . \tag{1}$$

Within the well the potential is flat and the field massless, $m_\phi^2 = 0$. Since realistic potentials are continuous, the wall potential must be regularized. Ref. [59] provides an example with a potential of the form [62]

$$V_{\rm B}(\phi) = \Lambda^4 \exp\left[\frac{\phi^2 - \bar{\phi}^2}{\Lambda^2}\right] + V_0 \,, \tag{2}$$

where Λ is the wall thickness and V_0 is a constant. The scalar mass is then

$$m_\phi^2 = 2\Lambda^2 \exp\left[-\frac{\bar{\phi}^2}{\Lambda^2}\right] , \tag{3}$$

which is exponentially suppressed if the well size exceeds the wall thickness, $\bar{\phi} \gg \Lambda$. For very thin walls, $\Lambda/\bar{\phi} \to 0$, we recover Eq. (1) with a massless field. We set $V_0 = -m_\phi^2 \Lambda^2/2$ to ensure $V_B(0) = 0$. The potential in Eq. (2) is radiatively stable, yields exponentially small masses, and supports matter-like oscillations at late times. These features make ϕ an ideal ultralight DM candidate.

Misalignment Production. The dynamics of a scalar field are governed by its equation of motion in the Friedmann–Lemaître–Robertson–Walker (FLRW) background. Initially displaced from the minimum of its potential, the field remains frozen by Hubble friction until the restoring force from the potential becomes comparable to the Hubble damping and drives it into motion. The Hubble term then damps the resulting oscillations.

Once the motion is confined near the potential minimum, the potential can be approximated as quadratic, leading to damped harmonic oscillations. This evolution constitutes the misalignment mechanism for DM production.

For now, we remain agnostic about the displacement's origin and denote by ϕ_i the field value at time t_i, when it is still held by Hubble friction. The homogeneous mode satisfies $\ddot{\phi} + 3H\dot{\phi} + V'(\phi) = 0$, where overdots and primes denote derivatives with respect to FLRW time and the field, respectively. In a radiation-dominated universe with temperature T, the Hubble parameter is $H = \sqrt{g_\star \pi^2/90}\, T^2/M_{\rm Pl}$, where $g_\star$ and $M_{\rm Pl}$ are the effective number of relativistic degrees of freedom and the reduced Planck mass. The temperature $T_\star$ at which the field begins to evolve is set by $H \simeq \sqrt{V'(\phi)/\phi}$, yielding $T_\star \sim \sqrt{m_\phi M_{\rm Pl}}\, \exp\!\big(\phi_i^2/4\Lambda^2\big)$.

We define the dimensionless field $\tilde{\phi} \equiv \phi/\Lambda$ and temperature $y \equiv \sqrt{H/m_\phi}$. For $\phi_i \lesssim \Lambda$, the field begins to move when $y \simeq 1$. The equation of motion then reads [63]

$$\frac{d^2\tilde{\phi}}{dy^2} = -\frac{1}{y^6}\frac{1}{\Lambda^2 m_\phi^2}\frac{\partial V}{\partial \tilde{\phi}}\,. \tag{4}$$

It is useful to identify the generic behavior of potentials that eventually lead to harmonic oscillations. For the purely harmonic case, $V_{\rm HO}(\phi) = m_\phi^2\phi^2/2$, the adiabatic invariant $I_{\rm HO} \equiv \phi^2/T^3$ remains conserved during the oscillatory phase [64], which begins at $T_{\rm HO} \sim \sqrt{m_\phi M_{\rm Pl}}$. Applying the virial theorem, the resulting relic abundance scales as $\Omega_\phi^{\rm HO} \propto \sqrt{m_\phi}\,\phi_i^2$. Assuming that the solution of Eq. (4) reaches the quadratic regime $V \simeq V_{\rm HO}$ at $y \ll 1$, we can express the relic abundance of ϕ as

$$\Omega_\phi h^2 = \left(\frac{g_*}{100}\right)^{-1/4}\left(\frac{m_\phi}{\rm eV}\right)^{1/2}\left(\frac{\Lambda}{10^{12}\,{\rm GeV}}\right)^2 f\!\left(\frac{\phi_i}{\Lambda}\right). \tag{5}$$

The function f can be obtained from the solution $\tilde{\phi}(y)$ of Eq. (4) with initial condition $\tilde{\phi}(y \gg 1) = \phi_i/\Lambda$, and it explicitly reads $f(\phi_i/\Lambda) \approx 0.16(y^6\tilde{\phi}'(y)^2 + \tilde{\phi}(y)^2)/y^3|_{y\ll 1}$. A viable wallion scenario must reproduce the observed DM relic abundance, $\Omega_{\rm DM}h^2 = 0.1200 \pm 0.0012$ [4].

Fig. 1 shows numerical results for f for the axion case, $V_{\rm axion}(\phi) = m_\phi^2\Lambda^2[1-\cos(\phi/\Lambda)]$, and for the wallion potential in Eq. (2). In both cases, the solution $\tilde{\phi}(y)$ depends only on ϕ_i/Λ. For $\phi_i \ll \Lambda$, both are approximately harmonic, yielding $f(\phi_i/\Lambda) \simeq 0.32\,(\phi_i/\Lambda)^2$. The axion case displays a sharp rise near its hilltop at $\phi_i = \pi\Lambda$, while the wallion yields a smaller, eventually constant result for $\phi_i \gtrsim \Lambda$, with $f(\phi_i/\Lambda) \simeq 0.14$ for $\phi_i \gtrsim 4\Lambda$ [65]. At large amplitudes, the Taylor-expanded wallion potential is dominated by higher-order terms $\sim \phi^{2n}$, with n increasing with ϕ_i. In this regime, the adiabatic invariant $I_{2n} \equiv \phi^{n+1}/T^3$ is conserved, and these terms induce anharmonic oscillations with $\rho_\phi \propto T^{6n/(1+n)}$ [66]. Consequently, $\sqrt{V'(\phi)/\phi} \propto T^{3(n-1)/(n+1)}$ redshifts faster than the Hubble rate for $n > 5$. As such terms dominate for $\phi \gtrsim 2.4\,\Lambda$, the field slow-rolls toward $\phi \simeq 2.4\,\Lambda$ before transitioning to matter-like oscillations.

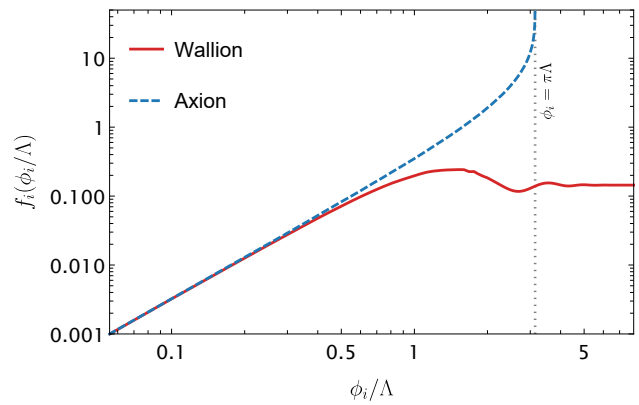

FIG. 1. Numerical evaluation of $f(x)$ from Eq. (5) for the axion (dashed blue) and wallion (solid red) potentials.

On the Initial Conditions. Cosmic inflation offers a natural origin for the initial wallion displacement. The field value at the end of inflation defines the initial condition ϕ_i entering Eq. (5). If the wallion potential is active during the inflationary phase, ϕ_i can become independent of the preinflationary value ϕ_0, provided inflation lasts long enough to erase any memory of it. This requires a number of e-folds N_e such that $\sqrt{N_e}\,(H_I/2\pi) \gg \max\{\phi_0,\, \min\{H_I^2/m_\phi,\, \Lambda\}\}$. In this *stochastic* scenario, the probability distribution [67, 68] of ϕ_i is given by

$$P_{\rm eq}(\phi_i) \propto \exp\left[-\frac{8\pi^2}{3H_I^4}\,V(\phi_i)\right]. \tag{6}$$

The relic density of ϕ then follows from the average

$$\Omega_\phi h^2\big|_{\rm stochastic} = \int d\phi_i\, P_{\rm eq}(\phi_i)\,\times\,\Omega_\phi h^2(\phi_i/\Lambda)\,, \tag{7}$$

where the relic density $\Omega_\phi h^2(\phi_i/\Lambda)$ for a given initial field value ϕ_i/Λ is given in Eq. (5).

If equilibration does not occur, the resulting distribution is Gaussian with standard deviation $\sqrt{N_e}\,H_I/(2\pi)$ and mean ϕ_0. In this *locked* scenario, where the field retains memory of its inflationary value, the relic abundance of ϕ follows Eq. (7) with $P_{\rm eq}(\phi_i)$ replaced by this Gaussian. If the preinflationary value is large, $\phi_0 \gg \sqrt{N_e}\,H_I/(2\pi)$, the relic density can instead be estimated by setting $\phi_i = \phi_0$ in Eq. (5).

To build intuition, we approximate the probability distribution in Eq. (6) with a window function that remains constant up to a cutoff in field amplitude. Explicitly, $P_{\rm eq}(\phi) \propto \Theta(\phi_{\rm cut} - |\phi|)$, where Θ denotes the Heaviside step function. The cutoff is set by $V(\phi_{\rm cut}) = 3H_I^4/(8\pi^2)$, which for the wallion potential yields

$$\frac{\phi_{\rm cut}^2}{\Lambda^2} = \ln\left[1 + \frac{3}{4\pi^2}\frac{H_I^4}{m_\phi^2\Lambda^2}\right]. \tag{8}$$

We identify two opposite scenarios. When $H_I \gg \sqrt{m_\phi \Lambda}$, the cutoff satisfies $\phi_{\rm cut} \gtrsim \Lambda$, and for sufficiently large H_I the relic density is well approximated by Eq. (5) with $f(\phi_i/\Lambda \gg 1) \simeq 0.14$. Requiring Λ values consistent with the observed relic abundance, this regime occurs for $H_I \gg 30\,(m_\phi/{\rm eV})^{3/8}\,{\rm GeV}$. Conversely, the cutoff satisfies $\phi_{\rm cut} \ll \Lambda$ when $H_I \ll \sqrt{m_\phi \Lambda}$. In this regime, the harmonic approximation holds, giving $f(\phi_i/\Lambda) \simeq 0.32\,(\phi_i/\Lambda)^2$. For $g_\star = 100$, the resulting relic abundance is $\Omega_\phi h^2 \simeq 8.1 \times 10^{-9}\,(H_I/{\rm GeV})^4\,(m_\phi/{\rm eV})^{-3/2}$. This corresponds to $m_\phi \simeq 1.7 \times 10^{-5}\,(H_I/{\rm GeV})^{8/3}\,{\rm eV}$, reproducing the well-known result for a free massive scalar [69].

Isocurvature. The wallion can generate isocurvature fluctuations since it is decoupled from radiation and unsourced by inflaton perturbations. Cosmic Microwave Background (CMB) data constrain their power to $\mathcal{P}_S < 7.6 \times 10^{-11}$ at the pivot scale $k = 0.002\,{\rm Mpc}^{-1}$ [4].

In the locked scenario, the isocurvature power spectrum can be approximated as $\mathcal{P}_S \approx \langle(\rho_\phi - \langle\rho_\phi\rangle)^2/\langle\rho_\phi\rangle^2\rangle$, where the average is taken over a Gaussian distribution with mean ϕ_i and standard deviation $H_I/(2\pi)$ [70–73]. For initial misalignments in the range $H_I/(2\pi) \ll \phi_i \lesssim \Lambda$, the CMB constraint implies an upper bound on the inflationary scale, $H_I/{\rm GeV} \lesssim 10^7\,(m_\phi/{\rm eV})^{-1/4}$, consistent with [69]. The opposite limit, $\phi_i < H_I/(2\pi)$, is excluded for $\phi_i \lesssim \Lambda$ since $\mathcal{P}_S \simeq 2$. Conversely, large misalignments $\phi_i \gtrsim \Lambda$ always evade the isocurvature bound in the locked scenario, as $f(\phi_i/\Lambda)$ saturates to a constant.

For the stochastic scenario, the isocurvature power spectrum is computed following the approach of [67, 74]. When $H_I^2 \ll \Lambda m_\phi$, existing results for quadratic potentials apply [69], whereas for $H_I^2 \gtrsim \Lambda m_\phi$ we numerically solve the Fokker–Planck equation for the wallion potential [75]. We find that $m_\phi \gtrsim 0.5\,{\rm GeV}$ is excluded by isocurvature constraints unless $H_I \gtrsim 10^{10}\,{\rm GeV}$.

Scenarios for Wallion Cosmology. In Fig. 2, we summarize the cosmologically viable parameter space. In the (m_ϕ, Λ^{-1}) plane, solid red and blue lines show $\Omega_\phi h^2 = 0.12$ isocontours for the locked and stochastic scenarios, respectively [76]. The blue lines converge to the red line for $\phi_i \gtrsim 4\Lambda$ for $H_I \gtrsim 10^3\,{\rm GeV}\,(m_\phi/{\rm eV})^{3/8}$. We also identify regions excluded by isocurvature constraints. For the locked scenario, we show bounds for different values of H_I with the region on the right of the colored green lines being excluded. For the stochastic scenario, the value of H_I for each point in the plane is identifed by the relic density constraint, and this leads to the exclusion of the purple region [77]. Shaded gray show constraints from the Lyman-α forest [78, 79] and black hole superradiance [80, 81]. The latter may not apply above a certain Λ^{-1} threshold, where ϕ self-interactions become relevant [82]. Additional constraints arise from modeling ultrafaint dwarf galaxies; the strongest, $m_\phi \gtrsim 8 \times 10^{-18}\,{\rm eV}$ [83, 84] (not shown), closes the gap between the Lyman-α and superradiance limits.

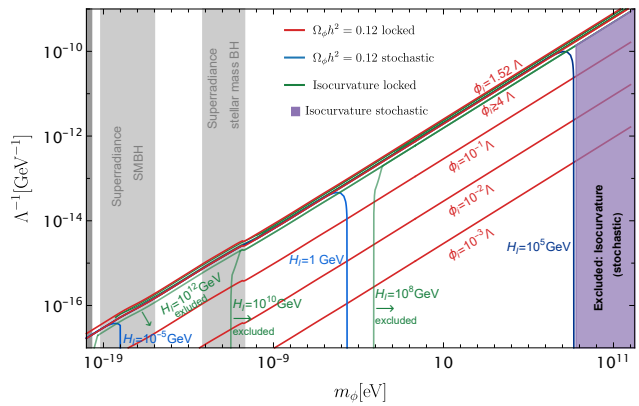

FIG. 2. Wallion parameter space in the (m_ϕ, Λ^{-1}) plane. See text for a detailed description.

A Plausible Origin: Istantons. We now turn to the microscopic origin of the wallion potential, showing that it can arise from instanton dynamics. Our approach parallels Ref. [85], where the Higgs potential was generated through instanton effects. We extend the SM by introducing a dark gauge group $SU(N)$ and a scalar field ϕ. The Lagrangian includes the following two operators:

$$\mathcal{L} \supset -\frac{1}{4g_d^2} G_{\mu\nu}G^{\mu\nu} + \frac{1}{4M^2}\phi^2 G_{\mu\nu}G^{\mu\nu}\,, \tag{9}$$

where g_d and $G_{\mu\nu}$ denote the dark gauge coupling and field-strength. The first term is the kinetic operator for the dark gauge bosons, while the dimension-6 contact interaction effectively redefines the gauge coupling

$$\frac{1}{g_{\rm eff}^2(\mu,\phi)} = \frac{1}{g_d^2(\mu)} - \frac{\phi^2}{M^2}\,, \tag{10}$$

where μ is the renormalization scale. Nonperturbative instanton effects can then generate the potential [86–90]

$$V_{\rm inst}(\phi) = K(\mu)\exp\left[-\frac{8\pi^2}{g_{\rm eff}^2(\mu,\phi)}\right]\,. \tag{11}$$

Up to the constant V_0, this reproduces the wallion potential in Eq. (2) with the identifications $\bar\phi^2 = M^2/g^2(\mu)$ and $\Lambda^2 = M^2/(8\pi^2)$. For $M^2 > 0$, the Lagrangian in Eq. (9) thus induces a field-space boundary at $|\phi| = \bar\phi$, beyond which the effective gauge coupling squared $g_{\rm eff}^2$, defined in Eq. (10), becomes negative. The sign and magnitude of $K(\mu)$ are determined by the instanton dynamics of the dark $SU(N)$. The existence of the boundary and the stability of the potential both require $K(\mu) > 0$.

We briefly comment on possible UV completions that generate the higher-dimensional operator in Eq. (9). One possibility is a mild breaking of the shift symmetry through interactions such as $\lambda\phi^2\eta^\dagger\eta$ or $\lambda\phi\bar\psi_1\psi_2$, where η and ψ_i are $SU(N)$-charged scalars and fermions, respectively. In the fermionic case, the linear coupling in ϕ can be forbidden by assigning suitable charges to ϕ and ψ_i under, for instance, a $\mathbb{Z}_2$ symmetry.

On the Possibility of SM interactions. All observable effects discussed so far, including the relic density and isocurvature signals, arise solely from gravitational interactions and wallion self-interactions encoded in the scalar potential of Eq. (2). Although couplings to SM fields are not required for the internal consistency of the framework, they open the appealing possibility of wallion detection in terrestrial experiments. If the heavy degrees of freedom generating the dimension-6 operator in Eq. (9) carry SM charges, additional higher-dimensional operators naturally emerge, such as

$$\mathcal{L} \supset \frac{c_F}{4M^2}\phi^2 F_{\mu\nu}F^{\mu\nu}\,, \tag{12}$$

where c_F is a coefficient determined by the UV completion and $F_{\mu\nu}$ denotes the electromagnetic field strength. This operator calls for a reassessment of the relic density analysis and threaten the naturalness of the wallion mass. In what follows, we focus on this example, keeping in mind that couplings to other SM fields may also arise.

We begin by addressing the issue of mass naturalness. Operators such as Eqs. (9) and (12) induce radiative corrections to the wallion mass. At one loop, this contribution can be estimated as $m^2_{\phi,\,\text{1-loop}} \sim \Lambda^4_{\text{UV}}/(512\pi^4\Lambda^2)$[91], where Λ_{UV} denotes a UV cutoff. Such corrections are generic in models with quadratically coupled ultralight DM [92–94]. We regard the instanton-induced potential as natural if $m^2_\phi > m^2_{\phi,\,\text{1-loop}}$. This condition is easily met when ϕ is decoupled from the SM, since Λ_{UV} can be arbitrarily low. In contrast, once the photon coupling in Eq. (12) is included, collider limits require $\Lambda_{\text{UV}} \gtrsim 100$ GeV. Whether this correction actually arises depends on the UV completion; for example, in frameworks such as Ref. [93], inspired by twin-Higgs models [95], the first nonvanishing contribution appears only at two loops. Thus, the naturalness issue is UV-sensitive rather than intrinsic to the wallion framework.

Interactions with photons also induce a thermal contribution to the wallion mass [96]

$$\Delta m^2_\phi(T) = c_F\alpha^2_{\text{em}}\frac{\pi^2}{3}\frac{T^4}{M^2}\,, \tag{13}$$

where α_{em} is the fine-structure constant. In a UV completion with a quartic coupling between the wallion and a heavy charged scalar, $\lambda\phi^2\eta^\dagger\eta$, the dimension-6 operators in Eqs. (9) and (12) acquire the same sign. Because the presence of a field-space boundary requires this sign to be opposite to that of the gauge kinetic term, the resulting squared thermal mass of the wallion is positive.

We assume instantaneous reheating, which produces a thermal bath characterized by a reheat temperature T_{rh}. Accordingly, we set $H_I = \sqrt{g_\star\pi^2/90}\,T^2_{\text{rh}}/M_{\text{Pl}}$. We further assume that the inflaton decays exclusively into SM states and restrict to reheating temperatures below the mass scale M associated with the operator in Eq. (12). Consequently, the dark sector remains cold already at reheating, and the wallion potential is present throughout. This also ensures that dark gluons never thermalize and thus do not contribute to dark radiation.

The wallion field evolution is governed by two sources: the potential in Eq. (2) and the thermal mass in Eq. (13). We first consider the locked inflationary scenario with $\phi(T_{\text{rh}}) = \phi_i$, assuming that the thermal mass dominates at T_{rh}. Assuming also that $\Delta m_\phi(T_{\text{rh}}) > H(T_{\text{rh}})$, the field then undergoes harmonic oscillations with a temperature-dependent mass, analogous to the QCD axion before confinement but following the scaling in Eq. (13). The ratio $\Delta m_\phi(T)/H(T)$ is temperature independent, so this oscillatory regime driven by the thermal mass $\Delta m_\phi(T)$ occurs only if $\Delta m_\phi(T_{\text{rh}}) > H(T_{\text{rh}})$, corresponding to $\Lambda^{-1} \gtrsim 8.7\times10^{-17}\sqrt{g_\star/c_F}\,\text{GeV}^{-1}$. The subsequent dynamics follow from conservation of the adiabatic invariant $I_T \equiv m_\phi(T)\phi(T)^2T^{-3}$, implying that the field amplitude redshifts as $\phi \propto T^{1/2}$. Eventually, the potential term dominates. If the preceding oscillatory phase lasts sufficiently long, the transition between the two regimes occurs while the wallion potential is approximately harmonic. Accordingly, the transition takes place at the temperature T_c defined by $\Delta m_\phi(T_c) = m_\phi$, where m_ϕ is the zero-temperature mass from Eq. (3). This is consistent provided $\phi_i/\Lambda \ll (T_{\text{rh}}/T_c)^{1/2}$. The subsequent evolution is matterlike, with a field amplitude at matter–radiation equality estimated as $\phi(T_{\text{eq}}) \simeq (T_{\text{eq}}/T_c)^{3/2}(T_c/T_{\text{rh}})^{1/2}\phi_i$. Matching this to the radiation energy density at that epoch, $m^2_\phi\phi(T_{\text{eq}})^2 = g_\star(T_{\text{eq}})(\pi^2/30)T^4_{\text{eq}}$, shows that the wallion reproduces the observed DM relic abundance for $\Lambda^{-1} \simeq 2\times10^{-3}\sqrt{c_F}(m_\phi/\text{eV})(\phi_i/\Lambda)^2T^{-1}_{\text{rh}}$.

The situation described above applies under specific circumstances, and there are possible exceptions. First, the thermal mass may be too small to permit oscillations ($\Delta m_\phi(T_{\text{rh}}) < H(T_{\text{rh}})$), with the field frozen until the wallion potential triggers its motion and the relic abundance given by Eq. (5), provided $T_{\text{rh}} > T_\star$. Another case occurs when the reheat temperature is small enough such that the wallion potential always dominates over the thermal mass. Assuming the wallion field at reheating satisfies $\phi_i \lesssim \Lambda$, the harmonic part of the potential drives its motion. If the reheat temperature is larger than $T_\star$ (i.e., $T_{\text{rh}} \gtrsim \sqrt{m_\phi M_{\text{Pl}}}$), the DM relic density constraint reads $\Lambda^{-1} \simeq (m_\phi/\text{eV})(\phi_i/\Lambda)(T_{\text{eq}}/T_{\text{rh}})^{1/2}T^{-1}_{\text{rh}}$. Finally, we address the stochastic scenario. Crucially, it is not possible to reproduce the relic density when $\Delta m_\phi(T_{\text{rh}}) > H(T_{\text{rh}})$ since the existence of the wallion potential during inflation requires the Hubble parameter H_I to be smaller than the dark confinement scale $\Lambda_D \approx \sqrt{m_\phi\Lambda}$. In the opposite case, the results for the stochastic scenario presented in Fig. 2 apply, as long as $T_{\text{rh}} > T_\star$ and $H_I \lesssim \Lambda_D$.

Fig. 3 summarizes the phenomenological constraints in the (m_ϕ, Λ^{-1}) plane, assuming wallion–photon inter-

actions with $c_F = 1$. The horizontal gray line marks the value of Λ for which $\Delta m_\phi(T_{\rm rh}) = H(T_{\rm rh})$. Above this line, we consider DM production impacted by $\Delta m_\phi(T)$ in the locked scenario and $T_{\rm rh} > T_c$. We set $\phi_i = \Lambda$ and at each point identify $T_{\rm rh}$ that reproduces the relic density. The solid red lines correspond to $T_{\rm rh} = 5\,{\rm MeV}$ and $T_{\rm rh} = 10^{15}\,{\rm GeV}$. The region to the left of the $T_{\rm rh} = 5\,{\rm MeV}$ line require larger initial misalignment ϕ_i because of the Big Bang Nucleosynthesis (BBN) constraints [97–99]. On the contrary, the region to the right of the $T_{\rm rh} = 10^{15}\,{\rm GeV}$ line requires smaller initial misalignment ϕ_i because Planck constraints on the energy scale of inflation [4]. The green shaded region indicates exclusion from isocurvature once we impose on each point a value of $T_{\rm rh}$ that reproduces the relic density for $\phi_i = \Lambda$.

Thermal scattering of bath particles produces wallions that can contribute to dark radiation or a hot DM subcomponent. Their production rate per unit volume is $\gamma_\phi(T) = (3c_F^2/\pi^3)T^8/M^4$, yielding an asymptotic comoving number density $Y_\phi^\infty \simeq 0.2\,(c_F^2/g_\star^{3/2})(M_{\rm Pl}T_{\rm rh}^3/M^4)$. Dark radiation is constrained by BBN [100–102] (for $m_\phi \lesssim 1\,{\rm MeV}$) and by the CMB [4] (for $m_\phi \lesssim 0.1\,{\rm eV}$), both requiring $\Delta N_{\rm eff} \lesssim 0.3$. Following Ref. [103], we obtain $\Delta N_{\rm eff} \simeq 75.6(Y_\phi^\infty)^{4/3}$[104], which in turn implies $\Lambda^{-1} \lesssim 4.6\,(g_\star^{3/8}/c_F^{1/2})M_{\rm Pl}^{-1/4}T_{\rm rh}^{-3/4}$. For $m_\phi \gtrsim 0.1\,{\rm eV}$, thermally produced wallions form a subdominant hot DM component. Requiring their mass density to stay below one percent of the observed DM abundance [105] yields $\Lambda^{-1} \lesssim 3.3\,(g_\star^{3/8}/c_F^{1/2})({\rm eV}/m_\phi)^{1/4}M_{\rm Pl}^{-1/4}T_{\rm rh}^{-3/4}$.

A quadratic coupling of ultralight DM to photons can be probed by a wide range of experiments [92, 96, 106–108]. We show in Fig. 3 with blue shaded regions constraints from tests of the weak equivalence principle [109, 110], time-variation in atomic transition frequencies [111], BBN [96, 112]. We also show with black dashed lines projections from upcoming atom interferometers [113, 114]. While not presented here, recent limits from sourcing in white dwarfs may also apply [115].

Finally, we discuss the region below the horizontal gray line where thermal effects are negligible. The red and blue curves denote the regions yielding successful DM production in the locked and stochastic inflationary scenarios, respectively. Each line corresponds to the maximal achievable coupling Λ^{-1} in the given scenario, obtained for $\phi_i \simeq 1.52\Lambda$ (locked) and $H_I = \Lambda_D$ (stochastic).

Conclusions. In this work, we introduced the wallion field with a potential bounded in field space and an exponentially suppressed and radiatively stable mass. The same potential drives matter-like oscillations at late times, making the wallion a compelling ultralight DM candidate. Unlike axion models with periodic potentials, the present-day energy density becomes independent of the inflationary misalignment once this exceeds a critical value. Intriguingly, this property is responsible for the suppression of isocurvature perturbations.

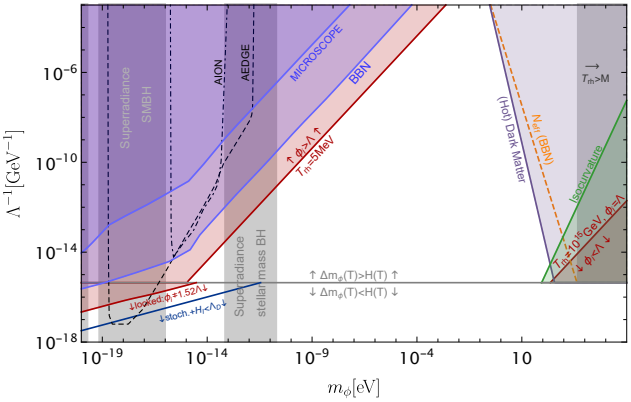

FIG. 3. Phenomenology of wallion-photon interactions in the (m_ϕ, Λ^{-1}) plane. See text for a detailed description.

We explored the possible origin from instanton effects in a confining dark gauge sector. This requires a dimension-6 quadratic coupling between the wallion and the gauge kinetic term. Remarkably, the framework operates entirely within the dark sector, without invoking interactions with SM fields. The framework becomes even more intriguing if the wallion also couples to visible particles. Such interactions can naturally emerge within the instanton setup when the heavy states responsible for the dimension-6 operator carry SM gauge charges. As we have shown, these couplings influence the cosmological evolution and relic density, while simultaneously opening a window for detection in forthcoming precision experiments such as AION and AEDGE.

This work sets the stage for several future developments. From the model-building perspective, a systematic study of UV completions that realize instanton-generated field-space boundaries represents an important next step. As discussed, the inclusion of SM interactions enriches the early-universe dynamics, and a detailed treatment of these effects will be essential to fully establish the framework. In a complementary direction, one may explore alternative origins of field-space boundaries, for instance from non-canonical kinetic terms in extra-dimensional constructions or from potentials induced for pseudo–Nambu–Goldstone bosons of non-compact, softly broken symmetries. These ideas are not limited to the exponential potential considered here but may apply more broadly to any setup that effectively behaves as an infinite potential well. From a phenomenological standpoint, field-space boundaries could also have far-reaching implications, including potential roles in inflationary model building, distinctive signatures in primordial non-Gaussianities, and modified superradiance bounds arising from wallion self-interactions with a sign opposite to that of axionic potentials. Altogether, these features identify field-space boundaries as a new and testable guiding principle for the origin of DM and scalar field dynamics in the early universe.

Acknowledgements. The authors thank Clifford Cheung, Jun'ya Kume, Martin Mojahed, Pablo Olgoso, Sebastian Schenk, Nudžeim Selimović, and Tien-Tien Yu for valuable feedback. This work was supported by Istituto Nazionale di Fisica Nucleare (INFN) through the Theoretical Astroparticle Physics (TAsP) project, and in part by the Italian MUR Departments of Excellence grant 2023-2027 "Quantum Frontiers". The work of M.B. was supported in part by the Italian Ministry of University and Research (MUR) through the PRIN 2022 project n. 20228WHTYC (CUP:I53C24002320006 and C53C24000760006). The work of V.V. was supported by the European Union's Horizon Europe research and innovation program under the Marie Skłodowska-Curie grant agreement No. 101065736, the Estonian Research Council grant RVTT7 and the Center of Excellence program TK202.

* mathias.becker@unipd.it
† francesco.deramo@pd.infn.it
‡ ville.vaskonen@pd.infn.it

[1] G. Jungman, M. Kamionkowski, and K. Griest, Phys. Rept. **267**, 195 (1996), arXiv:hep-ph/9506380.
[2] G. Bertone, D. Hooper, and J. Silk, Phys. Rept. **405**, 279 (2005), arXiv:hep-ph/0404175.
[3] J. L. Feng, Ann. Rev. Astron. Astrophys. **48**, 495 (2010), arXiv:1003.0904 [astro-ph.CO].
[4] N. Aghanim *et al.* (Planck), Astron. Astrophys. **641**, A6 (2020), [Erratum: Astron.Astrophys. 652, C4 (2021)], arXiv:1807.06209 [astro-ph.CO].
[5] A. Arbey and F. Mahmoudi, Prog. Part. Nucl. Phys. **119**, 103865 (2021), arXiv:2104.11488 [hep-ph].
[6] M. Cirelli, A. Strumia, and J. Zupan, (2024), arXiv:2406.01705 [hep-ph].
[7] N. Bozorgnia, J. Bramante, J. M. Cline, D. Curtin, D. McKeen, D. E. Morrissey, A. Ritz, S. Viel, A. C. Vincent, and Y. Zhang, Can. J. Phys. **103**, 671 (2025), arXiv:2410.23454 [hep-ph].
[8] E. Gildener, Phys. Rev. D **14**, 1667 (1976).
[9] S. Weinberg, Phys. Lett. B **82**, 387 (1979).
[10] G. F. Giudice, Naturally Speaking: The Naturalness Criterion and Physics at the LHC, in *Perspectives on LHC Physics*, edited by G. Kane and A. Pierce (2008) pp. 155–178, arXiv:0801.2562 [hep-ph].
[11] B. W. Lee and S. Weinberg, Phys. Rev. Lett. **39**, 165 (1977).
[12] H. Goldberg, Phys. Rev. Lett. **50**, 1419 (1983), [Erratum: Phys.Rev.Lett. 103, 099905 (2009)].
[13] R. J. Scherrer and M. S. Turner, Phys. Rev. D **33**, 1585 (1986), [Erratum: Phys.Rev.D 34, 3263 (1986)].
[14] M. Srednicki, R. Watkins, and K. A. Olive, Nucl. Phys. B **310**, 693 (1988).
[15] P. Gondolo and G. Gelmini, Nucl. Phys. B **360**, 145 (1991).
[16] G. Arcadi, M. Dutra, P. Ghosh, M. Lindner, Y. Mambrini, M. Pierre, S. Profumo, and F. S. Queiroz, Eur. Phys. J. C **78**, 203 (2018), arXiv:1703.07364 [hep-ph].
[17] L. Roszkowski, E. M. Sessolo, and S. Trojanowski, Rept. Prog. Phys. **81**, 066201 (2018), arXiv:1707.06277 [hep-ph].
[18] G. Arcadi, D. Cabo-Almeida, M. Dutra, P. Ghosh, M. Lindner, Y. Mambrini, J. P. Neto, M. Pierre, S. Profumo, and F. S. Queiroz, Eur. Phys. J. C **85**, 152 (2025), arXiv:2403.15860 [hep-ph].
[19] K. Ehret *et al.*, Phys. Lett. B **689**, 149 (2010), arXiv:1004.1313 [hep-ex].
[20] E. Arik *et al.* (CAST), JCAP **02**, 008, arXiv:0810.4482 [hep-ex].
[21] V. A. et al. (CAST), Nature Phys. **13**, 584 (2017), arXiv:1705.02290 [hep-ex].
[22] E. A. et al. (IAXO), JCAP **06**, 047, arXiv:1904.09155 [hep-ph].
[23] S. J. Asztalos *et al.* (ADMX), Phys. Rev. Lett. **104**, 041301 (2010), arXiv:0910.5914 [astro-ph.CO].
[24] T. B. et al. (ADMX), Phys. Rev. Lett. **124**, 101303 (2020), arXiv:1910.08638 [hep-ex].
[25] K. M. B. et al., Nature **590**, 238 (2021), arXiv:2008.01853 [quant-ph].
[26] D. A. et al. (CAPP), Phys. Rev. Lett. **128**, 181803 (2022), arXiv:2203.02105 [hep-ex].
[27] R. H. P. et al. (ABRACADABRA), Phys. Rev. Lett. **124**, 141802 (2020), arXiv:1910.08141 [hep-ex].
[28] A. A. C. et al. (DMRadio), Phys. Rev. D **105**, 022007 (2022), arXiv:2108.00012 [hep-ex].
[29] O. K. B. et al. (SHAFT), Phys. Rev. Lett. **130**, 121802 (2023), arXiv:2209.00609 [hep-ex].
[30] A. G. W. et al. (ORGAN), Phys. Rev. D **108**, 052004 (2023), arXiv:2308.12345 [hep-ex].
[31] W. Hu, R. Barkana, and A. Gruzinov, Phys. Rev. Lett. **85**, 1158 (2000), arXiv:astro-ph/0003365.
[32] A. Arvanitaki, S. Dimopoulos, S. Dubovsky, N. Kaloper, and J. March-Russell, Phys. Rev. D **81**, 123530 (2010), arXiv:0905.4720 [hep-th].
[33] D. J. E. Marsh and P. G. Ferreira, Phys. Rev. D **82**, 103528 (2010), arXiv:1009.3501 [hep-ph].
[34] P. W. Graham and S. Rajendran, Phys. Rev. D **84**, 055013 (2011), arXiv:1101.2691 [hep-ph].
[35] P. Svrcek and E. Witten, JHEP **06**, 051, arXiv:hep-th/0605206.
[36] F. Wilczek, Phys. Rev. Lett. **40**, 279 (1978).
[37] S. Weinberg, Phys. Rev. Lett. **40**, 223 (1978).
[38] J. Preskill, M. B. Wise, and F. Wilczek, Phys. Lett. B **120**, 127 (1983).
[39] L. F. Abbott and P. Sikivie, Phys. Lett. B **120**, 133 (1983).
[40] M. Dine and W. Fischler, Phys. Lett. B **120**, 137 (1983).
[41] R. D. Peccei and H. R. Quinn, Phys. Rev. Lett. **38**, 1440 (1977).
[42] R. D. Peccei and H. R. Quinn, Phys. Rev. D **16**, 1791 (1977).
[43] P. Arias, D. Cadamuro, M. Goodsell, J. Jaeckel, J. Redondo, and A. Ringwald, JCAP **06**, 013, arXiv:1201.5902 [hep-ph].
[44] D. J. E. Marsh, Phys. Rept. **643**, 1 (2016), arXiv:1510.07633 [astro-ph.CO].
[45] E. G. M. Ferreira, Astron. Astrophys. Rev. **29**, 7 (2021), arXiv:2005.03254 [astro-ph.CO].
[46] H.-Y. Schive, T. Chiueh, and T. Broadhurst, Nature Phys. **10**, 496 (2014), arXiv:1406.6586 [astro-ph.GA].
[47] P. Mocz, M. Vogelsberger, V. H. Robles, J. Zavala, M. Boylan-Kolchin, A. Fialkov, and L. Hernquist, Mon. Not. Roy. Astron. Soc. **471**, 4559 (2017),

arXiv:1705.05845 [astro-ph.CO].
[48] K. Van Tilburg, N. Leefer, L. Bougas, and D. Budker, Phys. Rev. Lett. **115**, 011802 (2015), arXiv:1503.06886 [physics.atom-ph].
[49] P. W. Graham, D. E. Kaplan, J. Mardon, S. Rajendran, and W. A. Terrano, Phys. Rev. D **93**, 075029 (2016), arXiv:1512.06165 [hep-ph].
[50] A. Hees, J. Guéna, M. Abgrall, S. Bize, and P. Wolf, Phys. Rev. Lett. **117**, 061301 (2016), arXiv:1604.08514 [gr-qc].
[51] A. Derevianko, Phys. Rev. A **97**, 042506 (2018), arXiv:1605.09717 [physics.atom-ph].
[52] M. S. Safronova, D. Budker, D. DeMille, D. F. J. Kimball, A. Derevianko, and C. W. Clark, Rev. Mod. Phys. **90**, 025008 (2018), arXiv:1710.01833 [physics.atom-ph].
[53] I. G. Irastorza and J. Redondo, Prog. Part. Nucl. Phys. **102**, 89 (2018), arXiv:1801.08127 [hep-ph].
[54] A. Arvanitaki and S. Dubovsky, Phys. Rev. D **83**, 044026 (2011), arXiv:1004.3558 [hep-th].
[55] R. Brito, V. Cardoso, and P. Pani, Lect. Notes Phys. **906**, pp.1 (2015), arXiv:1501.06570 [gr-qc].
[56] M. Baryakhtar, R. Lasenby, and M. Teo, Phys. Rev. D **96**, 035019 (2017), arXiv:1704.05081 [hep-ph].
[57] D. Baumann, H. S. Chia, and R. A. Porto, Phys. Rev. D **99**, 044001 (2019), arXiv:1804.03208 [gr-qc].
[58] K. K. Y. Ng, S. Vitale, O. A. Hannuksela, and T. G. F. Li, Phys. Rev. Lett. **126**, 151102 (2021), arXiv:2011.06010 [gr-qc].
[59] C. Cheung and I. Z. Rothstein, (2024), arXiv:2411.07380 [hep-ph].
[60] A. Nicolis and I. Z. Rothstein, SciPost Phys. **16**, 045 (2024), arXiv:2212.08976 [hep-th].
[61] G. Borghetto, A. Malhotra, G. Tasinato, and I. Zavala, Phys. Rev. D **112**, 023521 (2025), arXiv:2503.11628 [astro-ph.CO].
[62] This potential belongs to the broader EFT class with $V(\phi) = \exp(-\bar{\phi}^2/\Lambda^2)\,\Lambda^4 \sum_{n=0}^{\infty}(c_n/n!)(\phi^2/\Lambda^2)^n$ [59]. The potential in Eq. (2) corresponds to $c_n = 1$, and the periodic axion cosine potential to $c_n = (-1)^n n!/(2n)!$.
[63] Throughout this analysis, we approximate $g_* \simeq$ const.
[64] K. J. Bae, J.-H. Huh, and J. E. Kim, JCAP **09**, 005, arXiv:0806.0497 [hep-ph].
[65] Background field values $\phi > \Lambda$ do not necessarily invalidate the EFT interpretation of $V_B(\phi)$. The scale of new physics Λ limits the energy density, not the field amplitude, so the EFT remains valid as long as $V_B(\phi) < \Lambda^4$, or equivalently $\phi \lesssim \bar{\phi}$.
[66] M. S. Turner, Phys. Rev. D **28**, 1243 (1983).
[67] A. A. Starobinsky and J. Yokoyama, Phys. Rev. D **50**, 6357 (1994), arXiv:astro-ph/9407016.
[68] P. W. Graham and A. Scherlis, Phys. Rev. D **98**, 035017 (2018), arXiv:1805.07362 [hep-ph].
[69] T. Tenkanen, Phys. Rev. Lett. **123**, 061302 (2019), arXiv:1905.01214 [astro-ph.CO].
[70] J. Hamann, S. Hannestad, G. G. Raffelt, and Y. Y. Y. Wong, JCAP **06**, 022, arXiv:0904.0647 [hep-ph].
[71] M. P. Hertzberg, M. Tegmark, and F. Wilczek, Phys. Rev. D **78**, 083507 (2008), arXiv:0807.1726 [astro-ph].
[72] L. Visinelli and P. Gondolo, Phys. Rev. D **80**, 035024 (2009), arXiv:0903.4377 [astro-ph.CO].
[73] P. W. Graham and D. Racco, (2025), arXiv:2506.03348 [hep-ph].
[74] T. Markkanen, A. Rajantie, S. Stopyra, and T. Tenkanen, JCAP **08**, 001, arXiv:1904.11917 [gr-qc].
[75] The spectrum is obtained as a sum over modes with increasing spectral index. Unlike the quadratic case, higher-order terms contribute, and we observe numerical convergence after ~ 25 modes.
[76] In Fig. 2, we have $6 \lesssim \bar{\phi}/\Lambda \lesssim 15$ (see Eq. (3)).
[77] To ease the visualization, we interrupt the isocurvature exclusion lines before they approach the red one for $\phi_i \gtrsim 4\Lambda$ which is not subject to isocurvature bounds.
[78] T. Kobayashi, R. Murgia, A. De Simone, V. Iršič, and M. Viel, Phys. Rev. D **96**, 123514 (2017), arXiv:1708.00015 [astro-ph.CO].
[79] K. K. Rogers and H. V. Peiris, Phys. Rev. Lett. **126**, 071302 (2021), arXiv:2007.12705 [astro-ph.CO].
[80] M. J. Stott and D. J. E. Marsh, Phys. Rev. D **98**, 083006 (2018), arXiv:1805.02016 [hep-ph].
[81] H. Davoudiasl and P. B. Denton, Phys. Rev. Lett. **123**, 021102 (2019), arXiv:1904.09242 [astro-ph.CO].
[82] It is interesting to note that the predicted sign of the wallion self-interactions is opposite to that of the axion potential. This distinctive feature motivates a dedicated analysis of superradiance in the wallion scenario, which we leave for future work.
[83] N. Dalal and A. Kravtsov, Phys. Rev. D **106**, 063517 (2022), arXiv:2203.05750 [astro-ph.CO].
[84] S. May, N. Dalal, and A. Kravtsov, (2025), arXiv:2509.02781 [astro-ph.CO].
[85] H. Davoudiasl and M. Schnubel, Phys. Rev. D **112**, 075052 (2025), arXiv:2412.09675 [hep-ph].
[86] A. A. Belavin, A. M. Polyakov, A. S. Schwartz, and Y. S. Tyupkin, Phys. Lett. B **59**, 85 (1975).
[87] G. 't Hooft, Phys. Rev. Lett. **37**, 8 (1976).
[88] R. Jackiw and C. Rebbi, Phys. Rev. Lett. **37**, 172 (1976).
[89] C. G. Callan, Jr., R. F. Dashen, and D. J. Gross, Phys. Lett. B **63**, 334 (1976).
[90] M. Mariño, *Instantons and Large N: An Introduction to Non-Perturbative Methods in Quantum Field Theory* (Cambridge University Press, 2015).
[91] This estimate takes the coefficient of the operator in Eq. (12) with a loop suppression, uses the identification between M and Λ, and fixes the UV cutoff dependence by dimensional analysis.
[92] A. Banerjee, G. Perez, M. Safronova, I. Savoray, and A. Shalit, JHEP **10**, 042, arXiv:2211.05174 [hep-ph].
[93] C. Delaunay, M. Geller, Z. Heller-Algazi, G. Perez, and K. Springmann, (2025), arXiv:2507.12514 [hep-ph].
[94] D. Brzeminski, Z. Chacko, A. Dev, and A. Hook, Phys. Rev. D **104**, 075019 (2021), arXiv:2012.02787 [hep-ph].
[95] Z. Chacko, H.-S. Goh, and R. Harnik, Phys. Rev. Lett. **96**, 231802 (2006), arXiv:hep-ph/0506256.
[96] T. Bouley, P. Sørensen, and T.-T. Yu, JHEP **03**, 104, arXiv:2211.09826 [hep-ph].
[97] S. Hannestad, Phys. Rev. D **70**, 043506 (2004), arXiv:astro-ph/0403291.
[98] P. F. de Salas, M. Lattanzi, G. Mangano, G. Miele, S. Pastor, and O. Pisanti, Phys. Rev. D **92**, 123534 (2015), arXiv:1511.00672 [astro-ph.CO].
[99] N. Barbieri, T. Brinckmann, S. Gariazzo, M. Lattanzi, S. Pastor, and O. Pisanti, Phys. Rev. Lett. **135**, 181003 (2025), arXiv:2501.01369 [astro-ph.CO].
[100] T.-H. Yeh, K. A. Olive, and B. D. Fields, JCAP **03**, 046, arXiv:2011.13874 [astro-ph.CO].
[101] O. Pisanti, G. Mangano, G. Miele, and P. Mazzella, JCAP **04**, 020, arXiv:2011.11537 [astro-ph.CO].

[102] T.-H. Yeh, J. Shelton, K. A. Olive, and B. D. Fields, JCAP **10**, 046, arXiv:2207.13133 [astro-ph.CO].

[103] F. D'Eramo, F. Hajkarim, and A. Lenoci, JCAP **03**, 009, arXiv:2311.04974 [hep-ph].

[104] This procedure suffices for current constraints, while future CMB surveys will require a dedicated phase-space analysis (see, e.g., Refs. [116, 117]).

[105] F. D'Eramo and A. Lenoci, JCAP **10**, 045, arXiv:2012.01446 [hep-ph].

[106] D. Antypas *et al.*, (2022), arXiv:2203.14915 [hep-ex].

[107] C. Beadle, S. A. R. Ellis, J. Quevillon, and P. N. Hoa Vuong, Phys. Rev. D **110**, 035019 (2024), arXiv:2307.10362 [hep-ph].

[108] H. Kim, A. Lenoci, G. Perez, and W. Ratzinger, Phys. Rev. D **109**, 015030 (2024), arXiv:2307.14962 [hep-ph].

[109] S. Schlamminger, K. Y. Choi, T. A. Wagner, J. H. Gundlach, and E. G. Adelberger, Phys. Rev. Lett. **100**, 041101 (2008), arXiv:0712.0607 [gr-qc].

[110] P. Touboul *et al.* (MICROSCOPE), Class. Quant. Grav. **36**, 225006 (2019), arXiv:1909.10598 [gr-qc].

[111] A. Arvanitaki, J. Huang, and K. Van Tilburg, Phys. Rev. D **91**, 015015 (2015), arXiv:1405.2925 [hep-ph].

[112] S. Sibiryakov, P. Sørensen, and T.-T. Yu, JHEP **12**, 075, arXiv:2006.04820 [hep-ph].

[113] Y. A. El-Neaj *et al.* (AEDGE), EPJ Quant. Technol. **7**, 6 (2020), arXiv:1908.00802 [gr-qc].

[114] L. Badurina *et al.*, JCAP **05**, 011, arXiv:1911.11755 [astro-ph.CO].

[115] K. Bartnick, K. Springmann, S. Stelzl, and A. Weiler, (2025), arXiv:2509.25305 [hep-ph].

[116] F. D'Eramo and A. Lenoci, Phys. Rev. D **110**, 116028 (2024), arXiv:2410.21253 [hep-ph].

[117] M. Badziak and M. Laletin, JHEP **02**, 108, arXiv:2410.18186 [hep-ph].